HHS Public Access

Author manuscript

Magn Reson Med. Author manuscript; available in PMC 2020 June 01.

Published in final edited form as:

Magn Reson Med. 2019 June ; 81(6): 3662–3674. doi:10.1002/mrm.27681.

Patient specific prospective respiratory motion correction for efficient, free-breathing cardiovascular MRI

Michael A. Bush[1], **Rizwan Ahmad**[1,2,3], **Ning Jin**[4], **Yingmin Liu**[3], **Orlando P. Simonetti**[1,3,5,6,†]

[1]Biomedical Engineering, The Ohio State University, Columbus, OH, United States

[2]Electrical and Computer Engineering, The Ohio State University, Columbus, OH, United States

[3]Dorothy M. Davis Heart and Lung Research Institute, The Ohio State University, Columbus, OH, United States

[4]Cardiovascular MR R&D, Siemens Medical Solutions USA Inc, Columbus, OH, United States

[5]Internal Medicine, The Ohio State University, Columbus, OH, United States

[6]Radiology, The Ohio State University, Columbus, OH, United States

Abstract

Purpose—To develop a patient-specific respiratory motion correction technique with true 100% acquisition efficiency.

Methods—A short training scan consisting of a series of single heartbeat images, each acquired with a preceding diaphragmatic navigator, was performed to fit a model relating the patient-specific three-dimensional respiratory motion of the heart to diaphragm position. The resulting motion model was then used to update the imaging plane in real-time to correct for translational motion based on respiratory position provided by the navigator. The method was tested in a group of 11 volunteers with 5 separate free-breathing acquisitions: FB – no motion correction, FB-TF – free breathing with a linear tracking factor, Nav Gate – navigator gating, Nav Gate-TF – navigator gating with a tracking factor, and PROCO – prospective motion correction (proposed). Each acquisition lasted for 50 accepted heartbeats, where non-gated scans had a 100% acceptance rate, and gated scans accepted data only within a ±4 mm navigator window. Retrospective image registration was used to measure residual motion and determine the effectiveness of each method.

Results—PROCO reduced the range/RMSE of residual motion to 4.08±1.4/0.90±0.3mm, compared to 10.78±6.9/2.97±2.2mm for FB, 5.32±2.92/1.24±0.8mm for FB-TF, 4.08±1.6/0.93±0.4mm for Nav Gate, and 2.90±1.0/0.63±0.2mm for Nav Gate-TF. Nav Gate and Nav Gate-TF reduced scan efficiency to 48.84±9.31% and 54.54±10.12%, respectively.

Conclusion—PROCO successfully limited the residual motion in single-shot imaging to the level of traditional navigator gating, while maintaining 100% acquisition efficiency.

Keywords

motion correction; cardiovascular MRI; prospective motion correction; respiratory motion

[†]Correspondence to Orlando P. Simonetti, 460 W 12th Ave, Room 320, 43210, Columbus, OH, United States. (simonetti.9@osu.edu).

INTRODUCTION

Magnetic Resonance Imaging (MRI) has established itself as a safe and versatile imaging tool with a wide range of clinical applications. Due to relatively slow data acquisition, MRI is susceptible to motion-induced artifacts. These artifacts can lead to poor image quality, repeated scans, and decreased throughput and remain an obstacle to clinical utility. This problem is further amplified in cardiovascular magnetic resonance (CMR), where cardiac and respiratory motions coexist (1), and respiratory motion of the heart can range up to over 20 mm (2). Breath holding is commonly used to avoid respiratory effects; however, a significant fraction of patients cannot breath-hold. To allow free-breathing image acquisition, respiratory gated sequences have been developed to mitigate respiratory motion by “gating”, i.e., to restrict data acquisition to a narrow temporal window at end-expiration to capture all data during the same (or similar) phase of the respiratory cycle. To achieve this, a variety of methods are used to track the respiratory position, including respiratory bellows (3,4), navigator pulses (5), and self-gating signals (6). Although these techniques can reduce the effects of respiratory motion, they typically reject 50% to 70% of acquired data, thereby increasing scan time by a factor of 2 to 3 (7). These methods may also suffer from respiratory drift when the end-expiratory position changes over time, further reducing acquisition efficiency. Adaptive navigator windowing (end-expiratory tracking) follows the change in end-expiratory position (8,9); however, this combines data from disparate respiratory positions, which can lead to artifacts including blurring and ghosting.

More recently, self-navigation has allowed highly simplified continuous acquisitions, using signal fluctuations in the repeated scan of the same k-space data to track respiratory and cardiac motions. The resulting data are retrospectively binned into motion states (6,10–12). While this eliminates the need for a separate navigator gating pulse and is compatible with steady-state imaging, self-gating without motion correction reduces efficiency to the same degree as conventional gating when a single respiratory state is desired, as is the case for many CMR applications such as first-pass perfusion, LGE, and relaxation parameter mapping.

While rapid techniques allow the acquisition of an entire “single-shot” image within a single heartbeat, fast enough to avoid respiratory motion artifact, applications incorporating single-shot imaging often require registration across images for quantification purposes or to yield adequate SNR. For example, single-shot imaging for T1/T2/T2* mapping (13–16), first-pass perfusion (17,18), late gadolinium enhancement (LGE) (19), and diffusion tensor imaging (DTI) (20) utilize registration across multiple images for averaging or quantification. While retrospective image registration has been used to effectively correct for in-plane motion, post-hoc registration cannot correct for through-plane motion and may fail under exaggerated respiratory motion (21,22). This is especially important in parametric mapping and quantification techniques which assume that all residual motion is eliminated and each pixel is identical in anatomical position across multiple source images. In addition, retrospective registration does not always guarantee 100% efficiency; LGE techniques that employ motion correction to facilitate averaging generally acquire a large number of frames and eliminate those with poor registration prior to averaging (19).

Prospective motion correction techniques have been proposed to solve these issues; slice position and orientation are adjusted in real-time, reducing through-plane motion and allowing for increased acquisition efficiency (23). These techniques can use a variety of signals related to respiratory motion to guide the position of the imaging plane. The earliest and most commonly used methods employed a diaphragmatic navigator and non-patient-specific tracking factor (typically a 0.6 ratio of heart motion to diaphragm motion) to adapt slice position on-the-fly (2). This overly simplistic approach does not account for patient-to-patient variation, the complete three-dimensional nature of the respiratory motion of the heart, or previously observed hysteresis between inspiration and expiration (24,25). For these reasons, prospective tracking is generally applied only within a narrow navigator gating window (5mm to 8mm) to reduce residual motion (26); the narrower the gating window, the less efficient the acquisition is.

Techniques have been proposed to incorporate patient-specific motion models that increase efficiency and may eliminate the need for gating. One such method employed multiple navigators simultaneously acquired with 3D image volumes to train affine motion models; this requires significant setup time and image segmentation prior to affine registration for location-specific feature tracking (27). Multiple navigators placed on the heart also eliminate the possibility of myocardial imaging, given that the signal within the navigators may not recover prior to image data acquisition. In addition, this work was performed in segmented Cartesian imaging, where prospective slice tracking can induce ghosting as it cannot simultaneously correct for disparate motions in different organs (28).

More recent work has fit elliptical models in two dimensions to account for non-linear motion of the heart using a single diaphragmatic navigator and affine registered 2D frames as training data; however, fitting motion models in a 2D plane is generally an over-simplification of the full 3D motion of the heart (25). Additionally, affine registration requires accurate segmentation of the region of interest, e.g., the heart, as the chest wall and spinal column do not move in synchrony with the heart, increasing the time and complexity of the model training process.

The aim of this project is to develop a patient-specific prospective motion correction technique that is capable of characterizing three dimensional motion of the heart, able to adapt to respiratory hysteresis, does not require selective segmentation of training data to track specific regions of interest, and can be implemented with a single diaphragmatic navigator signal to allow for real-time updates of the scan plane on a beat by beat basis for single-shot imaging.

METHODS

The proposed method can be summarized as follows: first, a short training scan is performed to acquire snapshot images of the heart at various respiratory positions along with a diaphragmatic navigator. Retrospective nonrigid image registration across the snapshots is used to extract spatially resolved motion information. The translational motion within the region of interest is then fit to the navigator signal using fractional polynomial regression on a separate computer. The regression coefficients are sent to the scanner and applied during

real-time imaging, updating the central location of the image plane prior to each single-shot 2D acquisition.

Model Training

Fifty 2D single-shot gradient echo (Image Matrix: 140–182×192, FOV 400 mm, Temporal Window 240–326 ms, Bandwidth 898–1532 Hz/Px, TE 1.79 ms, TR 3.68–4.02 ms) training frames were acquired in two orthogonal views over multiple respiratory cycles as shown in Figure 1. Image parameters were varied to optimize the sequence for spatial and temporal resolution and diastolic timing on a per-subject basis. Many single-shot CMR applications are acquired in the short-axis view, hence our two orthogonal views included short-axis (SAX) and 2-chamber (2CH) views to most accurately capture heart motion in the image coordinate system, defined by X_i, Y_i, and Z_i. While the 4-chamber (4CH) view could be used as well, it is the most susceptible to through-plane motion and registration errors. To reduce cardiac motion, each single-shot acquisition was performed at end-diastole. Volunteers 1–6 were instructed to breathe naturally during the training phase, and volunteers 7–11 were instructed to take a deep breath at the beginning of training data acquisition, followed by natural breathing, to investigate whether training over a wider range of motion could improve model performance. A diaphragmatic navigator signal, n, preceded the center of k-space for each training frame by approximately 135 ms. Following data acquisition, motion of the heart was estimated using non-rigid image registration (21). As shown in Figure 2A, all frames were registered to an end-expiratory reference frame, producing deformation fields that characterized the motion of each pixel, as shown in Figure 2C. The resulting non-rigidly registered frames are shown in Figure 2B. To extract average translational motion within a manually defined region of interest (ROI), each deformation field was averaged within the same ROI to yield dY_i and dX_i from the SAX view, and dZ_i from the 2CH view, which represent motion of the ROI in the image coordinate system as described in Figure 1. This results in two data streams: $[n(k), dY_i(k), dX_i(k)]$ from the SAX view and $[n(k), dZ_i(k)]$ from the 2CH view, where $k = 1{:}50$ is the temporal index of training frames. As shown in Figure 3, these translations were transformed into the MRI physical coordinate system denoted as X_p, Y_p and Z_p, as both views are, in general, double-oblique to the MR physical coordinate system, and therefore each image coordinate system dimension has a vector component in all three physical coordinate system dimensions, with the summation of all dimensional components reflecting the full motion of the heart. To accommodate hysteresis, each set of $[n(k), dX_p(k), dY_p(k), dZ_p(k)]$ was classified as inspiratory or expiratory and the fractional polynomial regression, performed individually for X_p, Y_p and Z_p against the navigator, was likewise performed separately for inspiratory or expiratory states. Respiratory phase was determined simply from the sign of the derivative of the navigator curve. We chose fractional polynomial regression to model the nonlinear relationship between cardiac motion and navigator signal;compared to high-order polynomial regression, fractional polynomial regression is more robust to the errors at or slightly beyond the limits of training data (29). We define the cardiac motion in terms of navigator signal and its square-root:

$$d_j(k) = a_j + b_j n(k) + c_j \sqrt{n(k)} \quad [1]$$

where d_j represents the position of the heart along the jth dimension and a_j, b_j, and c_j represent model coefficients. The process is repeated for three different ortientations of j, i.e., $j \in [X_p, Y_p, Z_p]$. The resulting coefficients from both training views were summed to generate one composite model that explains translations of the ROI along X_p, Y_p, and Z_p as a function of navigator-based diaphragm position. Through-plane motion is implicitly captured by modeling in-plane translations in two-orthogonal views. Final regression coefficients were applied with a modified pulse sequence that updated slice position in real-time to correct for translational motion in three dimensions. The entire training phase lasted approximately 3 minutes, with the acquisition of training data comprising 2 minutes and another minute for model definition. Navigator setup time was not included in this estimation, as it applies to all navigator-based methods. PROCO sample code and data can be found at https://github.com/michaelbush1313/PROCO.

Testing in Healthy Volunteers

The method was tested in a group of 11 volunteers (4 female, 7 male, age 32.36±9.17). The study was approved by the local institutional review board, and informed written consent was obtained from all volunteers. All acquisitions were performed on a 3T scanner (MAGNETOM Tim Trio, Siemens Heathineers, Erlangen, Germany). Five separate free-breathing acquisitions were run in the following order;

- FB – free-breathing with no motion correction
- Nav Gate – navigator gating with a ±4 mm acceptance window
- PROCO – patient-specific prospective motion correction
- FB-TF – free-breathing with 0.6 tracking factor
- Nav Gate-TF, navigator gating with a ±4 mm window plus a 0.6 slice tracking factor

The same acquisition order was used in all volunteers and the scans were queued up to run consecutively without pause. Each method was tested in perpendicular short axis, 2-chamber and 4-chamber views for each volunteer. Image matrices varied by volunteer with imaging parameters identical to the training data resolution for each volunteer.

PROCO and FB-TF acquisitions prospectively update the imaging plane once per heartbeat in single-shot image acquisitions. FB-TF takes the product of the tracking factor and the difference between the current and reference diaphragm positions to shift the imaging plane in the superior-inferior direction. A fixed tracking factor of 0.6 was used; this value is commonly used in practice for prospective respiratory motion correction in cardiac imaging. In contrast, PROCO updates the imaging plane in all three orthogonal directions (not only

superior-inferior) based on patient-specific fractional polynomial regression coefficients that convert the current diaphragm position into displacements. Each acquisition lasted for 50 accepted heartbeats resulting in 50 single-shot GRE images at the same prescribed slice position. FB, FB-TF, and PROCO accepted all acquired images, and gated acquisitions (Nav Gate and Nav Gate-TF) accepted images acquired only when the diaphragm was within a ±4 mm window; adaptive gating to track the end expiratory position was applied in the two gated acquisitions. Any frames mistakenly accepted due to incorrect navigator echo readings were discarded; this occurred, e.g., when the edge detection algorithm incorrectly selected anatomy other then the lung-diaphragm interface, or when the search window was poorly defined.

Statistical Analysis

To analyze performance, all testing frames within each acquisition were retrospectively registered to measure residual motion using the process defined in Figure 2. The first frame in each acquisition was discarded, as PROCO's model begins with the second frame to allow for determination of respiratory phase from two consecutive navigator positions. To reduce errors associated with registering to a potentially errant frame, all frames are first registered to the first frame. Translations from each frame were binned and a frame from the most populated bin was selected as a reference. Original frames were then registered again to this reference, producing a set of $[dX(k), dY(k)]$ where $k = 2{:}50$. Note the loss of the subscript i, as each view is analyzed independently within its own 2D space. ROI's for this analysis covered the entire left ventricle in the short axis view, a mid-ventricular slice in the 2-chamber view, and the lateral myocardial wall in the 4-chamber view as shown in Supporting Information Figure S1; similar ROI's were used in each volunteer. The magnitude of the motion is defined as:

$$r(k) = \sqrt{dY^2(k) + dX^2(k)}, \quad [2]$$

where $r(k)$ represents a single measure of motion at each frame. To provide a measure of displacement over the duration of the scan, root mean squared error (RMSE) is defined as:

$$RMSE = \sqrt{\sum_{k=2}^{50} (r(k) - \bar{r})^2}, \quad [3]$$

where $\bar{r}$ represents the value of r averaged over all frames. As $r(k)$ is a magnitude measurement, the range is defined as:

$$range = \max(r(k)).$$

[4]

The acquisitions showing the smallest value of both range of $r(k)$ and magnitude of RMSE were deemed the best in terms of motion correction; this analysis was performed separately in each of the 3 views, producing a single measure of RMSE and range for each volunteer and view (N = 33). Measurements from all views and volunteers were then combined for a single average measure of residual motion for each method. In addition, a spatial similarity index (SSIM) was assessed across all frames for each method following retrospective image registration. The SSIM of the FB acquisition with retrospective registration only was compared against combined prospective/retrospective correction (FB-TF, PROCO, Nav-Gate and Nav-Gate-TF) (30). SSIM provided a metric that was used to assess the improvements afforded by prospectively correcting in and through-plane motion. Gating efficiency, maximum range of navigator positions and estimated heart rate were also recorded for each acquisition, where gating efficiency was the percentage of acquired frames that were accepted.

RESULTS

Compared to FB acquisitions, Nav Gate-TF provided the greatest reduction in both the range and RMSE of residual motion, followed sequentially by PROCO, Nav Gate and FB-TF, as shown in Figure 4. Range and RMSE for all methods were found to have unequal variance, and a group-wise Steel-Dwass test to maintain significance found FB greater than, and Nav-Gate-TF smaller than all methods for both range and RMSE. In an individual comparison, Welch's test found a statistically significant ($p \leq 0.05$) difference between FB-TF and PROCO measurements for both RMSE and range with p-values of 0.019 and 0.032, respectively. FB acquisitions showed the lowest mean SSIM compared to all other methods, as shown in Table 1; SSIM measurements showed equal variance, and a Tukey-Kramer test found only a significant difference between FB and Nav-Gate-TF methods. In an individual t-test comparison, PROCO had significantly higher SSIM than FB with p-value 0.012. PROCO was comparable to gated methods while maintaining 100% scan efficiency, in contrast with 48.84±9.31% and 54.54±10.12% efficiency for Nav Gate and Nav Gate-TF respectively. Heart rate was not correlated with residual motion. Maximum navigator ranges (mimimum to maximum diaphragm position across each acquisition) are reported in Table 2; distributions had equal variance, and ANOVA testing found no significant differences between breathing patterns encountered during each of the different techniques. Means and standard deviations of maximum navigator ranges for each volunteer are reported in Supporting Information Table S1. A standard t-test found no significant difference in navigator ranges between FB-TF and PROCO acquisitions. Additionally, no difference was found in residual motion in PROCO acquisitions between volunteers trained with a maximal breath (N = 5) vs. natural breathing (N = 6).

Average maximal X_p, Y_p and Z_p physical translations applied during PROCO acquisitions were 3.51±3.07, 3.38±2.05, and 12.09±7.25 mm, respectively, and are displayed in Table 3. For comparison, average maximal Z_p translations during FB-TF acquisitions measured 15.12±7.61 mm (TF-Z_p in Table 3). In addition, maximal error between FB-TF and PROCO models are shown in Table 3. As FB-TF cannot distinguish between respiratory phase, error is calculated with respect to PROCO inspiratory (TF-EI) and expiratory models (TF-EE) and measured 3.41±2.32 and 4.21±3.02 mm, respectively. X_p and Y_p translations represent error associated with FB-TF as well, as FB-TF does not account for motion in these dimensions.

Figure 5 shows a sample analysis for a single volunteer in the short axis view; the magnitude of residual motion $r(k)$ is plotted with respect to the 49 analyzed heartbeats for all 5 methods alongside the singular value for RMSE. In this example, free-breathing motion was significant, reaching an RMSE of 3.72 mm and a range of 15.76 mm. PROCO reduced this motion to within the range of navigator gating while accepting every consecutive frame (RMSE – 0.61 mm, range – 3.27 mm), in contrast to the FB-TF acquisition which showed significant residual motion (RMSE – 2.44 mm, range – 11.92 mm). A video of all methods applied in the all views for this volunteer is provided in the Supporting Information Video S1. A sharp spike in residual motion due to a deep breath can be seen at the end of the FB-TF acquisition in Figure 5, which is clearly visible in Supporting Information Video S1 as well. Portions of the recorded navigator positions for all acquisitions in Figure 5 are provided in Supporting Information Figure S2. Sample frames shown in Figure 6 from a separate volunteer demonstrate the effects of respiratory motion and the efficacy of each technique. A single frame at end-expiration (EE) from FB acquisitions is shown for each view, along with frames at end-inspiration for all views and non-gated methods. Significant through and in-plane motion is visible in all end-inspiratory FB frames, illustrating the need for prospective correction in lieu of retrospective methods that cannot correct for this motion. Inspiration induced errors include absence of papillary muscles in the SAX view, nearly indistinguishable left-ventricular myocardium in the 4CH view, and loss of clarity of inferior myocardium in the 2CH view. While FB-TF does significantly reduce this motion, in-plane motion remains in both the short axis and four chamber views which translates to through-plane motion in the two-chamber view, significantly degrading image quality. PROCO reduces in-plane motion in all three views, and therefore reduces through-plane motion as well; frames are similar in comparison to frames acquired at end-expiration. A complete residual motion analysis of the short axis view for all 11 volunteers is included in the Supporting Information Figure S3.

DISCUSSION

We have developed a novel method for prospective motion correction in CMR, modeling the relationship between diaphragm position and the three-dimensional respiratory motion of the heart and correcting for that motion in real time in single-shot imaging. Our patient-specific technique reduces in-plane and through-plane motions while maintaining 100% acquisition efficiency. PROCO has the potential to dramatically improve the efficiency and reliability of CMR by reducing acquisition time and reducing misregistration across images acquired during free-breathing. Respiratory phase specific fractional polynomial regression models are capable of adapting to a wide variety of breathing patterns and account for hysteresis

between inspiratory and expiratory motion of the heart. The use of non-rigid image registration to train the model removes the need for pre-emptive segmentation of a specific ROI, by using the entire FOV for the registration process. While manual selection of an ROI following registration is still required for motion extraction, this allows for location specific feature tracking, and creates an opportunity for prospective tracking of particular anatomical features. In addition, our method only requires a single navigator and knowledge of the previous navigator to calculate and update the new image position in real time, with a feedback latency of less than 10 ms for the tested navigator technique and scanner hardware.

Our summary results in Figure 4 show that PROCO reduced residual motion to that of traditional navigator gating, significantly reducing motion across all volunteers while maintaining 100% acquisition efficiency. Navigator range was also found to be statistically similar across all methods, confirming that breathing pattern did not vary significantly between methods. Our results do show that FB-TF using the generally applied 0.6 tracking factor in the superior-inferior direction was appropriate in some cases, and Nav-Gate-TF offered a small improvement over Nav-Gate alone. FB-TF also showed significant improvement over pure free-breathing, implying that for some individuals this generic tracking factor is accurate. However, our results showed considerable residual motion when the simple linear tracking factor was applied in some volunteers, particularly those with large ranges of respiratory motion as seen in the Supporting Information Figure S3 for volunteers 6, 7 and 11 and Supporting Information Video S1. Table 3 shows the maximal applied translations averaged across all FB-TF and PROCO acquisitions, along with the associated difference between FB-TF and PROCO models for Z_p translations, as FB-TF only corrects for Z_p motion. FB-TF is not subject specific and cannot account for hysteresis effects, which could explain the differences observed. In addition to this difference in Z_p motion estimation, FB-TF ignores X_p and Y_p translations which are non-zero and show high standard deviations due to subject-subject variation.

Motion can occur in multiple dimensions, and the relationship between diaphragm position and heart motion can change with inspiration and expiration as illustrated in Figure 3, which shows the multi-dimensional and respiratory phase specific motion of a sample volunteer; a simple linear tracking factor in the superior-inferior direction did not accurately characterize this motion. In the presence of respiration induced motion of the heart that is highly subject-specific, PROCO performed consistently well across all volunteers. PROCO acquisitions were not performed immediately after model training, providing some evidence that it is resistant to changes in breathing patterns; however, it is also likely that breathing patterns remained largely similar in our group of volunteers as navigator ranges were not different between any of the applied methods. Additional work is required to evaluate the stability and effectiveness of PROCO models over time, perhaps including PROCO acquisitions at the beginning, middle and end of the exam while randomizing the order of motion correction methods, which was not done in this study.

FB-TF proved less accurate than PROCO in some circumstances, exhibiting several outliers. This concept is illustrated in Figure 5, where FB-TF performed relatively well until this subject took a deep breath at the end of the acquisition, skewing the results. In addition, the effects of through-plane motion are clearly visible in the end-inspiratory frames of FB as

shown in Figure 6, particularly in the two-chamber view. This amount of motion can significantly alter the anatomy within the field of view; when the anatomy changes from frame to frame due to through-plane motion, it is impossible for retrospective image registration to recover this information. While this particular volunteer did not take a similar deep breath during the PROCO acquisition however, when considering our results on a group scale and the data showing that navigator range did not change over time between acquisitions, we feel that the study represents a fair comparison between the techniques.

This study was performed in a cohort of healthy volunteers, free of any cardiac or respiratory disease. The majority of these subjects demonstrated a shallow, steady breathing pattern that is compatible with traditional navigator gated methods, with relatively stationary end-expiratory position and high gating efficiency. Under these conditions, we have assumed that PROCO models remain valid throughout the exam, but further testing must be performed in patient populations that show greater variability in respiratory patterns. A significant problem with navigator gated techniques can be respiratory drift, where the end-expiratory position changes over time; this can cause increased scan times. However, if the gating acceptance window is allowed to dynamically adapt to a changing end-expiratory diaphragm position, this implies that data are being accepted at different respiratory positions; if the reference position for slice tracking is allowed to shift as well, then respiratory adaptation will certainly lead to slice-slice mismatch. While adaptive windowing was enabled during our gated acquisitions, the end-expiratory position never drifted more than 2 mm in this cohort of normal volunteers. However, if PROCO is adequately trained on the full range of respiratory motion, then no adaptive gating window should be required. PROCO is robust to drifts in respiratory position within the training range; however, should the hysteresis loop of motion change during the acquisition some errors in motion estimation will occur. Our results, however, would suggest that this did not occur in our study population. Figure 7 shows sample model training for four separate volunteers, and further illustrates the importance of patient-specific motion modeling, as each volunteer is drastically different in terms of respiratory motion and 3-dimensional motion of the heart. Each model is plotted only over the full range of binned respiratory phases acquired during the training phase. Volunteers 1, 5 and 6 were not asked to take a deep breath during training, and represent the full range of shallow to deep breathing we observed in our study. Volunteer 8 was instructed to take a deep breath during training, and tidal range can be seen as a smaller percentage of this range. Volunteer 1 shows hysteresis in the Z direction under tidal breathing, as does Volunteer 6 in the X and Y directions. Likewise, Volunteer 8 shows hysteresis within the tidal range and is able to account for a wider range of motion given the trained deep breath. Trained deep breathing also allows for improved coverage of inspiratory and expiratory range; volunteer 5 shows incomplete characterization of inspiratory and expiratory curves due to rapid jumps in navigator position, whereas Volunteer 8 shows complete characterization. However, in this study no significant difference in PROCO efficiency was found between volunteers trained under normal breathing vs. instructed deep breathing. Future work could explore both training and testing under conditions of normal tidal breathing vs. coached breathing in order to explore the importance of training over the full range of respiratory motion.

Given the extremely shallow breathing shown in Volunteer 5, it is likely that some misclassification of inspiration vs. expiration occurred, as Nyquist rate is effectively violated. Other methods for tracking respiratory position could be combined with PROCO, offering higher temporal sampling and other potential advantages over diaphragmatic navigators. Respiratory bellows, for example, have the advantage of not interrupting the pulse sequence but require additional setup time. Optical cameras have been proposed as a calibration free method for tracking respiratory motion, but are generally expensive and require location specific installations (31,32). Pilot tone signals have been proposed as an alternative method for measuring cardiac and respiratory signals, have a one-time setup calibration, and can be integrated directly into the pulse sequence design (33,34). If acquired and analyzed in real-time, self-gating signals could be utilized as well, eliminating the need for additional hardware. However, in volunteers with such shallow breathing, inspiratory and expiratory models converge to be nearly identical with shifted ranges of training data; the difference between each model is minimal and our models are still accurate, though a simple linear tracking factor is sufficient.

Each method was compared with non-rigid image registration by evaluating SSIM over all acquired frames as shown in Table 1, with the assumption being that if spatial similarity is high, then motion correction has performed adequately. FB showed the lowest SSIM value, followed by FB-TF, PROCO, Nav-Gate and Nav-Gate-TF. The addition of prospective correction improved spatial similarity, implying that retrospective correction alone cannot account for all motion related inconsistencies.

Limitations and Future Directions

A potential source of error in our method lies in the training data itself; in the presence of significant through-plane motion, image content for a given view can change over the respiratory cycle, leading to possible registration errors, particularly when the subjects were asked to breathe deeply. While the current method has proven capable of estimating bulk in-plane motion, in future work we propose the use of low-resolution, 3D volumes for training, which would account for through-plane motion assuming the volumes are acquired in a rapid, single heart beat fashion to mitigate intraview respiratory motion. In addition, we have not considered rotations in this work; however, rotational respiratory motion of the heart is generally small (35), and can be corrected with retrospective registration assuming bulk through-plane motion has been corrected prospectively and through-plane rotations are limited. Further improvements to the training process are currently being developed, where translations from the two orthogonal views that share a common axis, Y_i, are pooled together, creating a single data stream of: $[n(k), dX_i(k), dY_i(k), dZ_i(k)]$, where $dY_i(k)$ includes data from both SAX and 2CH views. Another limitation to this work is the need to acquire training data as a separate scan. Training consisted of 100 total acquired heartbeats, 50 frames for each orthogonal view. However, this number was arbitrarily chosen and no attempt was made to determine the minimal number of training frames required. This work represents a feasibility study, and several steps could be taken to improve the efficiency of model development. The training sequence could be optimized to acquire both orthogonal views within a single end-diastolic period with two navigators, further reducing training time. While the training data are currently exported to a separate workstation for model

fitting, this step can be incorporated onto the scanner software. In addition, while ROI's for model definition are currently selected manually, automatic ROI placement will be implemented in the future by centering the training images on the ROI for automatic extraction.

There are a wide range of cardiac imaging applications that could benefit from PROCO, including T1/T2/T2* mapping, perfusion, late gadolinium enhancement (LGE), and diffusion tensor imaging (DTI). Myocardial T1 and T2 mapping, and some T2* mapping techniques (15,16) require multiple source images acquired at varying inversion recovery (IR), T2 prep times, or echo times to be perfectly overlaid in order to perform pixel by pixel parametric fitting; slice misregistration results in errors in fitting and inaccurate estimations. Breath-holds and navigator gating are not always feasible for these techniques. MOLLI T1 mapping schemes require source images to be acquired from consecutive heartbeats after an IR pulse, implying that all source images must be acquired within a single breath hold, and navigator gating could indefinitely prolong the acquisition until the correctly timed heartbeat falls within the gating window. T2 mapping is more readily adaptable to navigator gating; however, scan time can still increase dramatically with its use (22). Breath-holding limits the acquisition time of these techniques, reducing the number of sampled points for parameter estimation and decreasing accuracy of the fit. The development of free-breathing, prospectively motion corrected techniques would allow for increased sampling of the T1, T2, or T2* recovery curves, potentially improving the accuracy and precision of the measurement. Recent work has shown the benefits of prospective motion correction in parametric mapping techniques with the application of a 0.6 tracking factor (36), which could be further improved with PROCO as we have shown in our results. While PROCO is most readily applicable to these single-shot imaging techniques, it could also be combined with segmented imaging techniques acquired with non-Cartesian k-space trajectories such as radial (37) and spiral (38) that are inherently robust to motion artifacts.

Likewise, single-shot, motion-corrected LGE requires multiple source images acquired over multiple heartbeats and relies on retrospective in-plane correction to minimize slice mismatch (19). Gating (rejection of frames) is not applicable to first-pass perfusion imaging, and retrospective motion correction is unable to correct for through-plane motion. PROCO would allow for continuous perfusion image acquisition while minimizing in-plane and through-plane motion. DTI is an emerging technique that is limited by long scan times; acquisition efficiency could be greatly improved with the use of prospective motion correction (20). PROCO is readily applicable to such techniques and could significancly improve efficiency while reducing both through and in-plane motion.

CONCLUSION

We have developed a patient-specific, prospective motion correction method (PROCO) that can accurately characterize three-directional, respiratory phase specific motion of the heart and correct for this in real-time by adjusting the center of the slice-plane. PROCO was capable of reducing residual motion in multiple orthogonal views to a similar degree as navigator gating while maintaining 100% data acquisition effeciency. This method is particularly relevant to single-shot CMR techniques such as T1 and T2 mapping, first-pass

perfusion, single-shot LGE with averaging, and DTI. PROCO can improve imaging efficiency and mitigate slice-mismatching, potentially improving the efficiency and performance of these and other techniques based on single-shot imaging.

Supplementary Material

Refer to Web version on PubMed Central for supplementary material.

ACKNOWLEDGEMENTS

OPS and RA receive research support from Siemens Healthineers. OPS receives funding support from The Robert F. Wolfe and Edgar T. Wolfe Foundation. MB is supported by Award Number TL1TR001069 from the National Center for Advancing Translational Sciences. This work was additionally supported by the National Institute of Biomedical Imaging and Bioengineering (R21 EB026657). The content is solely the responsibility of the authors and does not necessarily represent the official views of the National Institutes of Health.

REFERENCES

1. Andre JB, Bresnahan BW, Mossa-Basha M, Hoff MN, Smith CP, Anzai Y, Cohen WA. Toward Quantifying the Prevalence, Severity, and Cost Associated With Patient Motion During Clinical MR Examinations. J. Am. Coll. Radiol 2015;12:689–95. doi: 10.1016/j.jacr.2015.03.007. [PubMed: 25963225]
2. Wang Y, Riederer SJ, Ehman RL. Respiratory Motion of the Heart: Kinematics and the Implications for the Spatial Resolution in Coronary Imaging. Magn. Reson. Med 1995;33:713–719. doi: 10.1002/mrm.1910330517. [PubMed: 7596276]
3. Wang Y, Christy PS, Korosec FR, Alley MT, Grist TM, Polzin JA, Mistretta CA. Coronary MRI with a Respiratory Feedback Monitor: The 2D Imaging Case. Magn. Reson. Med 1995;33:116–121. doi: 10.1002/mrm.1910330118. [PubMed: 7891525]
4. Santelli C, Nezafat R, Goddu B, Manning WJ, Smink J, Kozerke S, Peters DC. Respiratory Bellows Revisited for Motion Compensation: Preliminary Experience for Cardiovascular MR. Magn. Reson. Med 2011;1103:1098–1103. doi: 10.1002/mrm.22687.
5. Ehman RL, Felmlee JP. Adaptive technique for high-definition MR imaging of moving structures. Radiology 1989;173:255–263. doi: 10.1148/radiology.173.1.2781017. [PubMed: 2781017]
6. Larson AC, Kellman P, Arai A, Hirsch GA, McVeigh E, Li D, Simonetti OP. Preliminary investigation of respiratory self-gating for free-breathing segmented cine MRI. Magn. Reson. Med 2005;53:159–168. doi: 10.1002/mrm.20331. [PubMed: 15690515]
7. Jhooti P, Keegan J, Firmin DN. A fully automatic and highly efficient navigator gating technique for high-resolution free-breathing acquisitions: Continuously adaptive windowing strategy. Magn. Reson. Med 2010;64:1015–1026. doi: 10.1002/mrm.22491. [PubMed: 20593372]
8. Deshpande V, Finn J, Ruehm S, Laub G, Krishnam M. Non-contrast MR Angiography of the heart and great vessels using SSFP with non-selective excitation. Proc. 14th Sci. Meet. Int. Soc. Magn. Reson. Med 2006;14:1935.
9. Krishnam MS, Tomasian A, Deshpande V, Tran L, Laub G, Finn JP, Ruehm SG. Noncontrast 3D steady-state free-precession magnetic resonance angiography of the whole chest using nonselective radiofrequency excitation over a large field of view: Comparison with single-phase 3D contrast-enhanced magnetic resonance angiography. Invest. Radiol 2008;43:411–420. doi: 10.1097/RLI.0b013e3181690179. [PubMed: 18496046]
10. Piccini D, Littmann A, Nielles-Vallespin S, Zenge MO. Respiratory self-navigation for whole-heart bright-blood coronary MRI: Methods for robust isolation and automatic segmentation of the blood pool. Magn. Reson. Med 2012;68:571–579. doi: 10.1002/mrm.23247. [PubMed: 22213169]
11. Pang J, Bhat H, Sharif B, Fan Z, Thomson LEJ, Labounty T, Friedman JD, Min J, Berman DS, Li D. Whole-heart coronary MRA with 100% respiratory gating efficiency: Self-navigated three-dimensional retrospective image-based motion correction (TRIM). Magn. Reson. Med 2014;71:67–74. doi: 10.1002/mrm.24628. [PubMed: 23401157]

12. Feng L, Axel L, Chandarana H, Block KT, Sodickson DK, Otazo R. XD-GRASP: Golden-angle radial MRI with reconstruction of extra motion-state dimensions using compressed sensing. Magn. Reson. Med 2016;75:775–788. doi: 10.1002/mrm.25665. [PubMed: 25809847]
13. Xue H, Shah S, Greiser A, Guetter C, Littmann A, Jolly MP, Arai AE, Zuehlsdorff S, Guehring J, Kellman P. Motion correction for myocardial T1 mapping using image registration with synthetic image estimation. Magn. Reson. Med 2012;67:1644–1655. doi: 10.1002/mrm.23153. [PubMed: 22135227]
14. Giri S, Shah S, Xue H, Chung YC, Pennell ML, Guehring J, Zuehlsdorff S, Raman SV., Simonetti OP. Myocardial T2 mapping with respiratory navigator and automatic nonrigid motion correction. Magn. Reson. Med 2012;68:1570–1578. doi: 10.1002/mrm.24139. [PubMed: 22851292]
15. Jin N, Da Silveira JS, Jolly MP, Firmin DN, Mathew G, Lamba N, Subramanian S, Pennell DJ, Raman SV., Simonetti OP. Free-breathing myocardial T2 mapping using GRE-EPI and automatic Non-rigid motion correction. J. Cardiovasc. Magn. Reson 2015;17:1–12. doi: 10.1186/s12968-015-0216-z. [PubMed: 25589308]
16. Kellman P, Xue H, Spottiswoode BS, et al. Free-breathing T2* mapping using respiratory motion corrected averaging. J. Cardiovasc. Magn. Reson 2015;17:1–8. doi: 10.1186/s12968-014-0106-9. [PubMed: 25589308]
17. Bidaut LM, Vallee JP. Automated registration of dynamic MR images for the quantification of myocardial perfusion. J. Magn. Reson. Imaging 2001;13:648–655. [PubMed: 11276113]
18. Gallippi CM, Kramer CM, Hu YL, Vido DA, Reichek N, Rogers WJ. Fully automated registration and warping of contrast-enhanced first-pass perfusion images. J. Cardiovasc. Magn. Reson 2002;4:459–469. doi: 10.1081/JCMR-120016384. [PubMed: 12549233]
19. Kellman P, Larson AC, Hsu LY, Chung YC, Simonetti OP, McVeigh ER, Arai AE. Motion-corrected free-breathing delayed enhancement imaging of myocardial infarction. Magn. Reson. Med 2005;53:194–200. doi: 10.1002/mrm.20333. [PubMed: 15690519]
20. Nguyen C, Fan Z, Xie Y, Pang J, Speier P, Bi X, Kobashigawa J, Li D. In vivo diffusion-tensor MRI of the human heart on a 3 tesla clinical scanner: An optimized second order (M2) motion compensated diffusion-preparation approach. Magn. Reson. Med 2016;76:1354–1363. doi: 10.1002/mrm.26380. [PubMed: 27550078]
21. Chefd'hotel C, Hermosillo G, Faugeras O. Flows of diffeomorphisms for multimodal image registration. Proc. - Int. Symp. Biomed. Imaging 2002;2002–1:753–756. doi: 10.1109/ISBI.2002.1029367.
22. Giri S, Shah S, Xue H, Chung Y, Pennell ML, Guehring J, Zuehlsdorff S, Raman SV, Simonetti OP. Myocardial T2 Mapping with Respiratory Navigator and Automatic Nonrigid Motion Correction. Magn. Reson. Med 2012;1578:1570–1578. doi: 10.1002/mrm.24139.
23. McConnell MV, Khasgiwala VC, Savord BJ, Chen MH, Chuang ML, Manning WJ, Edelman RR. Prospective adaptive navigator correction for breath-hold MR coronary angiography. Magn. Reson. Med 1997;37:148–152. doi: 10.1002/mrm.1910370121. [PubMed: 8978644]
24. Taylor AM, Keegan J, Jhooti P, Firmin DN, Pennell DJ. Calculation of a subject-specific adaptive motion-correction factor for improved real-time navigator echo-gated magnetic resonance coronary angiography. J. Cardiovasc. Magn. Reson 1999;1:131–8. [PubMed: 11550345]
25. Burger I, Meintjes EM. Elliptical subject-specific model of respiratory motion for cardiac MRI. Magn. Reson. Med 2013;70:722–731. doi: 10.1002/mrm.24502. [PubMed: 23045163]
26. Firmin D, Keegan J. Navigator echoes in cardiac magnetic resonance. J. Cardiovasc. Magn. Reson 2001;3:183–93. doi: 10.1081/JCMR-100107467. [PubMed: 11816615]
27. Manke D, Nehrke K, Börnert P. Novel prospective respiratory motion correction approach for free-breathing coronary MR angiography using a patient-adapted affine motion model. Magn. Reson. Med 2003;50:122–131. doi: 10.1002/mrm.10483. [PubMed: 12815687]
28. Nehrke K, Börnert P. Prospective correction of affine motion for arbitrary MR sequences on a clinical scanner. Magn. Reson. Med 2005;54:1130–1138. doi: 10.1002/mrm.20686. [PubMed: 16200564]
29. Royston P, Altman DG. Regression Using Fractional Polynomials of Continuous Covariates: Parsimonious Parametric Modelling. Appl. Stat 1994;43:429. doi: 10.2307/2986270.

30. Wang Z, Bovik AC, Sheikh HR, Simoncelli EP. Image Quality Assessment: From Error Visibility to Structural Similarity. IEEE Trans. Image Process. 2004;13:600–612. doi: 10.1109/TIP.2003.819861. [PubMed: 15376593]

31. Auboiroux V, Petrusca L, Viallon M, Muller A, Terraz S, Breguet R, Montet X, Becker CD, Salomir R. Respiratory-gated MRgHIFU in upper abdomen using an MR-compatible in-bore digital camera. Biomed Res. Int 2014;2014. doi: 10.1155/2014/421726.

32. Schaerer J, Fassi A, Riboldi M, Cerveri P, Baroni G, Sarrut D. Multi-dimensional respiratory motion tracking from markerless optical surface imaging based on deformable mesh registration. Phys. Med. Biol 2011;57:357–373. doi: 10.1088/0031-9155/57/2/357. [PubMed: 22170786]

33. Schroeder L, Wetzl J, Maier A, Lauer L, Bollenbeck J, Fenchel M, Speier P. A Novel Method for Contact-Free Cardiac Synchronization Using the Pilot Tone Navigator. Proc. Intl. Soc. Mag. Reson. Med 24 2016:0410. doi: 10.1002/mrm.25858.

34. Wetzl J, Schroeder L, Forman C, Lugauer F, Rehner R, Fenchel M, Maier A, Hornegger J, Speier P. Feasibility Study: Free-Breathing 3-D CINE Imaging with Respiratory Gating Based on Pilot Tone Navigation. Proc. 24th Annu. Meet. ISMRM (ISMRM 2016) 2016:3–5. doi: 10.1007/s10334-015-0487-2.

35. Shechter G, Ozturk C, Resar JR, McVeigh ER. Respiratory motion of the heart from free breathing coronary angiograms. IEEE Trans. Med. Imaging 2004;23:1046–1056. doi: 10.1109/TMI.2004.828676. [PubMed: 15338737]

36. Weingärtner S, Roujol S, Akçakaya M, Basha TA, Nezafat R. Free-breathing multislice native myocardial T1 mapping using the slice-interleaved T1 (STONE) sequence. Magn. Reson. Med 2015;74:115–124. doi: 10.1002/mrm.25387. [PubMed: 25131652]

37. Glover G, Pauly J. Projection reconstruction techniques for reduction of motion effects in MRI. Magn. Reson. Med 1992;28:275–289. doi: 10.1002/mrm.1910280209. [PubMed: 1461126]

38. Jan-Ray L, John MP, Thomas JB, Norbert JP. Reduction of motion artifacts in cine MRI using variable-density spiral trajectories. Magn. Reson. Med 1997;37:569–575. [PubMed: 9094079]

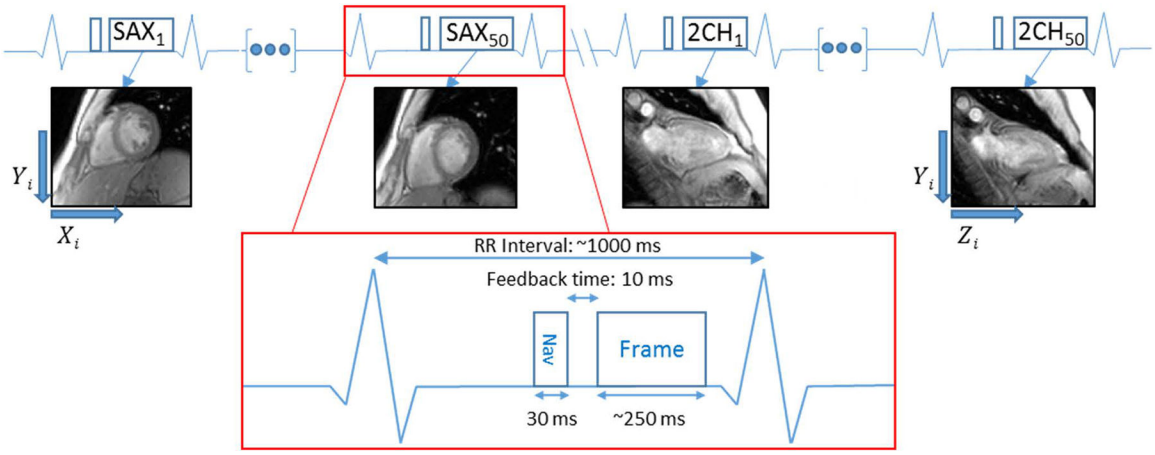

Figure 1.

Training sequence diagram. The Frame block represents a low resolution single shot GRE image acquired 50 times in both the SAX and 2CH training views, resulting in 100 total slices and 100 corresponding navigator positions used for training. Orthogonal training views allow for description of a 3D space, with SAX comprising the dY_i and dX_i components, and 2CH the dZ_i component and shared dY_i.

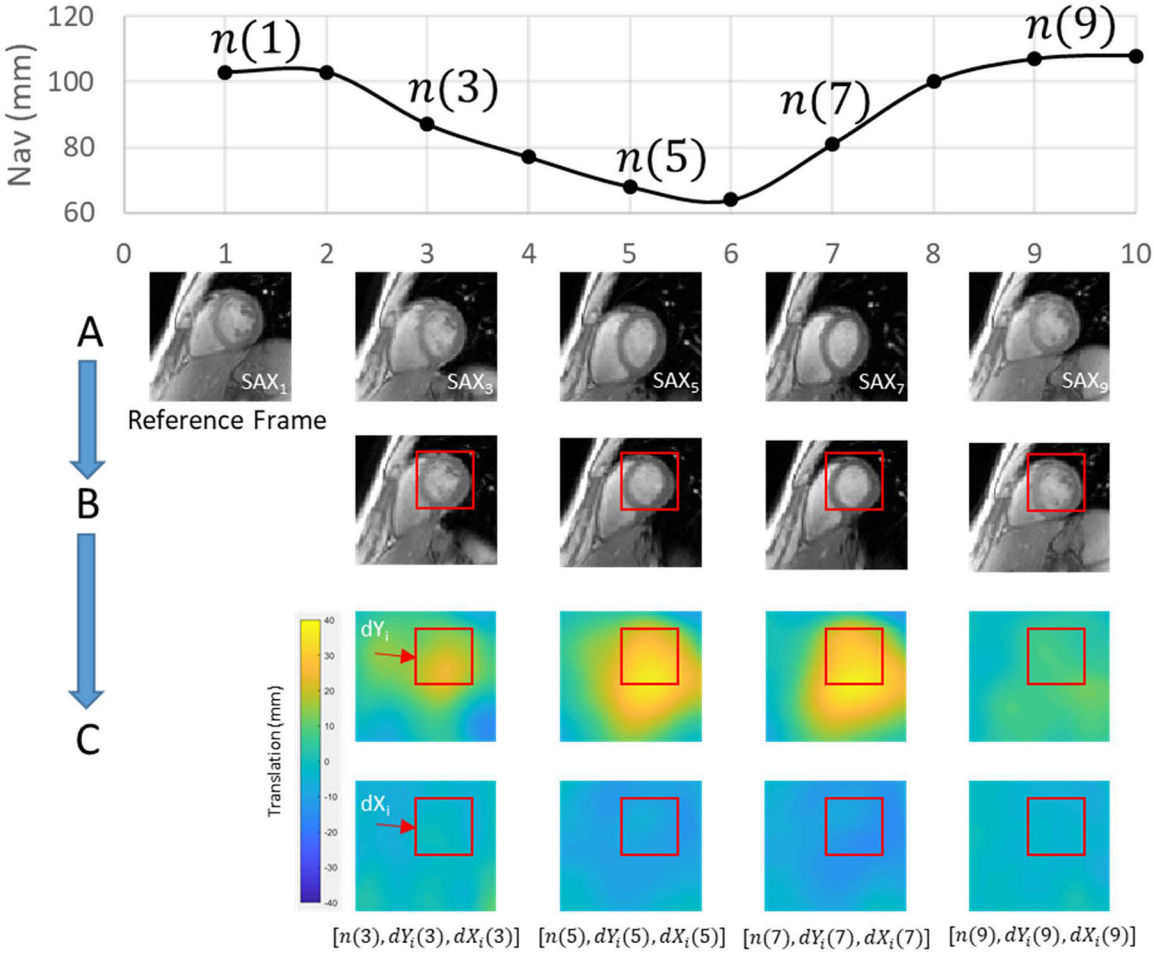

Figure 2.

Motion extraction. (A) Source images are acquired once per heartbeat over 50 heartbeats for each training view. (B) Source images are registered to a reference frame acquired at end-expiration using non-rigid image registration. (C) Deformation fields produced from non-rigid registration are averaged within a single ROI to extract a set of navigator, dY_i and dX_i positions. This process is repeated on the orthogonal 2CH view, producing a set of navigator and dZ_i positions.

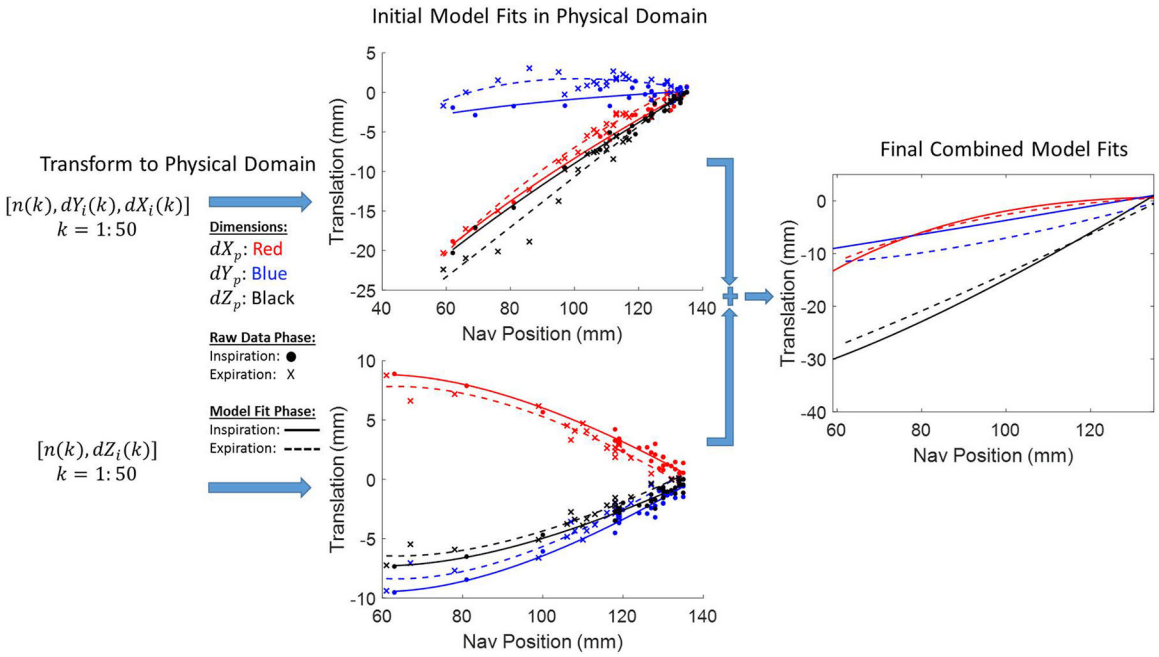

Figure 3.

Motion extraction from training data produces sets of [$n(k)$, $dY_i(k)$, $dX_i(k)$] from the SAX view and [$n(k)$, $dZ_i(k)$] from the 2CH view for k = 1:50, where $n(k)$ represents the navigator position and $dX_i(k)$, $dY_i(k)$, $dZ_i(k)$ the position of the heart in the image coordinate system. Each set is classified as inspiratory or expiratory phase and transformed into the MR physical coordinate system (denoted by the subscript "p"). Data within each dimension and phase are then characterized with fractional polynomial regressions with respect to navigator position; coefficients from corresponding models in both orthogonal planes are then summed to produce final parameters for use with our modified pulse sequence.

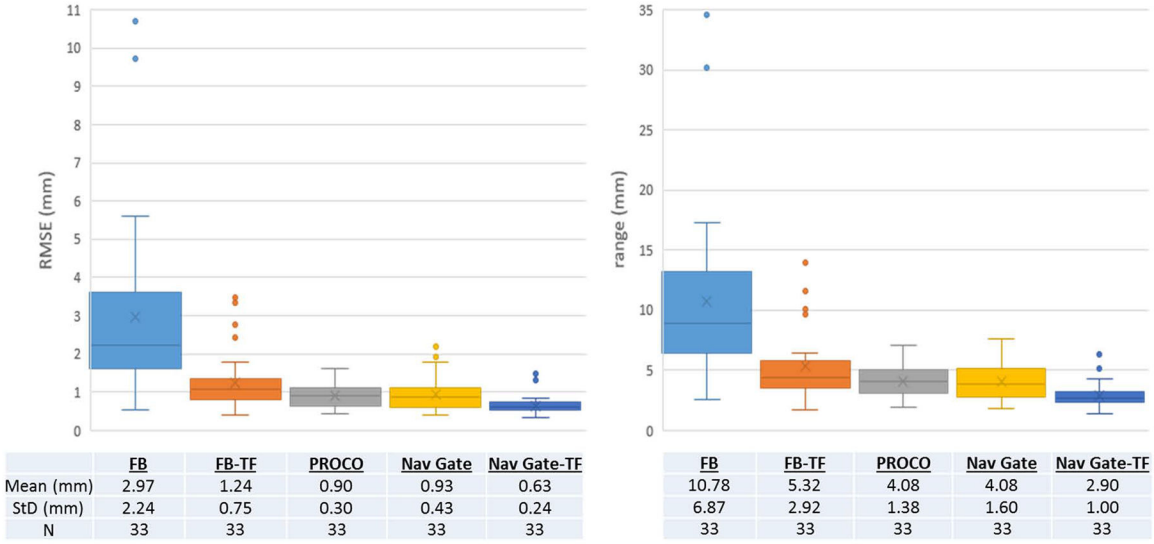

	FB	FB-TF	PROCO	Nav Gate	Nav Gate-TF
Mean (mm)	2.97	1.24	0.90	0.93	0.63
StD (mm)	2.24	0.75	0.30	0.43	0.24
N	33	33	33	33	33

FB	FB-TF	PROCO	Nav Gate	Nav Gate-TF
10.78	5.32	4.08	4.08	2.90
6.87	2.92	1.38	1.60	1.00
33	33	33	33	33

Figure 4.

Summary residual motion analysis. All techniques reduce motion compared to FB acqusitions, with Nav Gate-TF performing the best at the expense of increased scan time. PROCO performs similarly to navigator gating, while maintaining 100% acceptance rate, and reduces residual motion compared to the application of a purely linear 0.6 superior-inferior tracking factor (FB-TF).

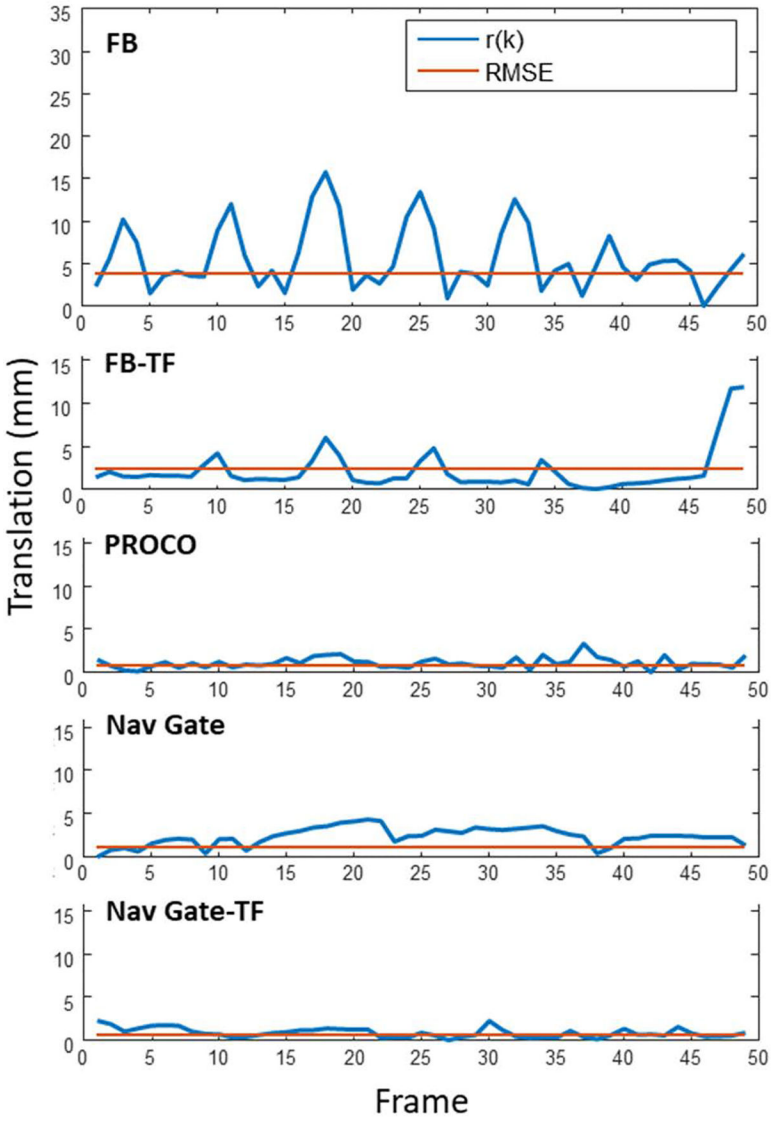

Figure 5.

Sample residual motion analysis. $r(k)$ represents the magnitude of residual motion over the course of 49 acquired frames, and RMSE the root mean squared error of $r(k)$, which are both significant under free-breathing (FB) conditions. The application of a simple lnear tracking factor of 0.6 in the superior-inferior direction (FB-TF) reduces this motion, but is susceptible to errors under varied breathing patterns. PROCO reduces the motion to a similar degree as navigator gated techniques (Nav Gate and Nav Gate-TF); however, PROCO frames are acquired consecutively, and both navigator gated techniques accept frames only at end-expiration, greatly reducing efficiency.

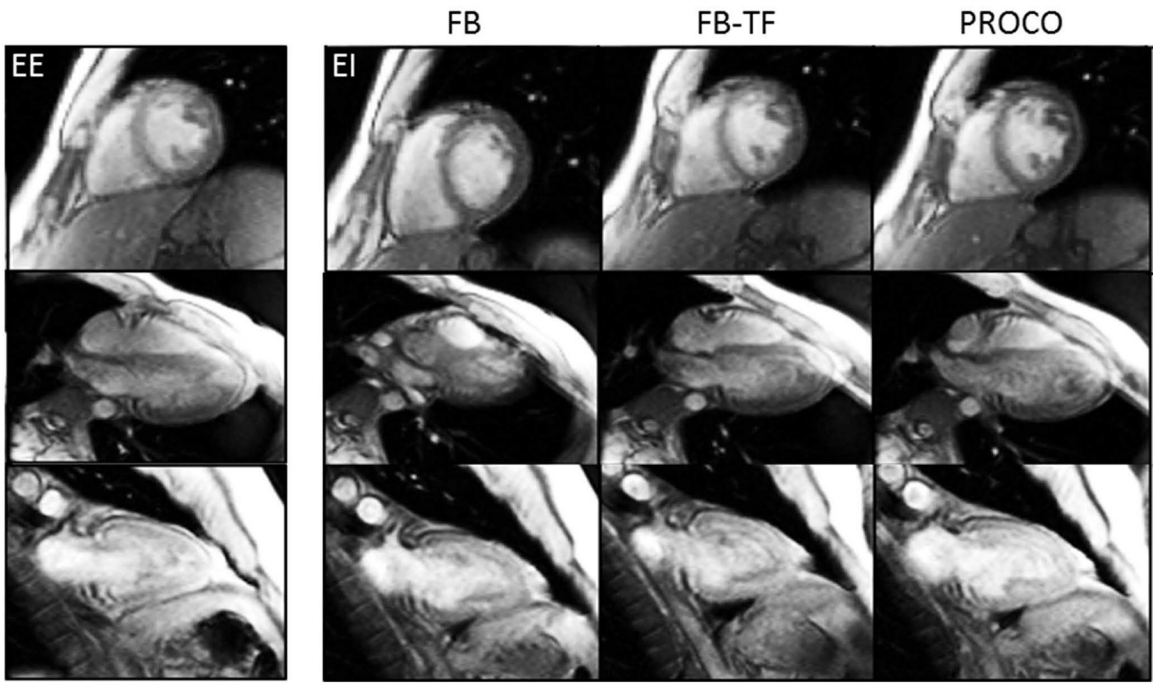

Figure 6.

Sample method comparison. Single-shot frames at end-inspiration (EI) are shown for the three free-breathing methods and 3 acquired views, along with frames at end-expiration (EE) from FB acquisitions for reference. Severe in and through-plane motion can be seen in free-breathing (FB) frames, which is largely eliminated in PROCO scans. FB-TF does reduce motion, but some residual in-plane motion can be seen in the SAX and 4CH end-inspiratory frames, which correspond to drastic through plane motion in the corresponding 2CH end-inspiratory frames.

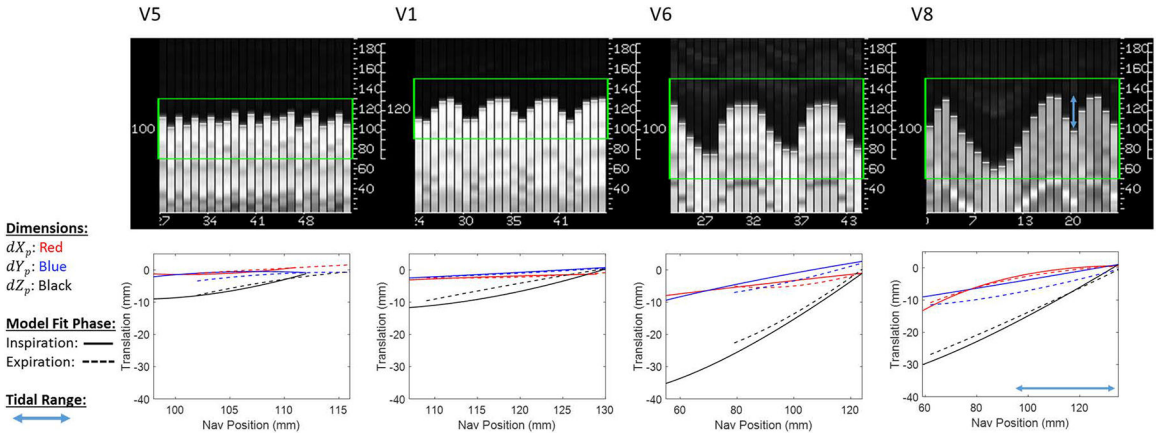

Figure 7.

Sample motion models plotted over the range of binned respiratory positions. Models shown are from a wide range of respiratory patterns, including shallow breathing (V5), medium depth breathing (V1) and consistent deep breathing (V6). V8 illustrates a trained deep breath followed by tidal breathing. Shallow breathing shows highly linear motion in the Z_p direction and minimal X_p and Y_p translations, whereas deep breathing shows hysteresis in the Z_p direction and significant X_p and Y_p translations. Trained breathing in V8 shows improved characterization of inspiratory and expiratory curves, which could improve model accuracy in case of deep breathing during the acquisition.

Table 1.

All frames from each method are retrospectively registered and analyzed for structural similarity index (SSIM). Mean SSIM reflects the average spatial agreement with a reference frame, and is lowest in FB acquisitions, which implies retrospective image registration alone cannot achieve similar image quality to other methods.

	FB	FB-TF	PROCO	Nav-Gate	Nav-Gate-TF
Mean (mm)	0.63	0.69	0.70	0.70	0.73
Std (mm)	0.12	0.13	0.12	0.11	0.11

Table 2.

Maximum navigator range was recorded for every acquisition and averaged within each method (N = 33, with 11 volunteers and 3 averages). No significant difference was found on a group scale, implying that respiratory patterns remained consistent between methods.

	FB	FB-TF	PROCO	Nav-Gate	Nav-Gate-TF
Mean (mm)	25.7	25.2	24.3	27.3	26.7
Std (mm)	13.4	12.7	11.6	11.6	15.0

Table 3.

Maximal applied PROCO translations were calculated and averaged across each PROCO acquisition in X_p, Y_p and Z_p directions, along with maximal Z_p translations for each FB-TF acquisition (TF-Z_p). Maximal error between FB-TF and PROCO models were calculated based on projected TF-Z_p and the corresponding PROCO applied Z_p for both inspiratory (TF-EI) and expiratory (TF-EE) models, as FB-TF cannot distinguish between respiratory phases.

	PROCO-X_p	**PROCO-Y_p**	**PROCO-Z_p**	**TF-Z_p**	**TF-EI**	**TF-EE**
Mean (mm)	3.51	3.38	12.09	15.11	3.41	4.21
Std (mm)	3.07	2.05	7.25	7.61	2.32	3.02